PHILOSOPHICAL TRANSACTIONS OF THE ROYAL SOCIETY A MATHEMATICAL, PHYSICAL & ENGINEERING SCIENCES

The Concentration and Pressure Dependent Diffusion of Carbon Dioxide in Nitrile Rubbers

B. J. Briscoe, D. Gritsis and D. Liatsis

Phil. Trans. R. Soc. Lond. A 1992 **339**, 497-519
doi: 10.1098/rsta.1992.0049

The concentration and pressure dependent diffusion of carbon dioxide in nitrile rubbers

By B. J. Briscoe[1], D. Gritsis[2] and D. Liatsis[1]

[1] *Department of Chemical Engineering and Chemical Technology, Imperial College of Science, Technology and Medicine, London, U.K.*

[2] *Department of Chemical and Biochemical Engineering, University College, London, U.K.*

Contents

	PAGE
1. Introduction	498
2. Materials and equipment	499
3. Experimental techniques	499
4. Experimental results	502
5. Preliminary analysis	503
6. Data processing strategy	507
7. Results of the parameter estimation procedure	509
8. Discussion of results	512
9. Conclusions	514
Appendix A	514
Appendix B	515
Appendix C	516
References	518

The paper reports the results of an experimental and associated analytical study of the time dependent adsorption of carbon dioxide gas into two nitrile elastomers. The mass gas sorption has been measured using a device based on a vibrating reed to a weight fraction accuracy of *ca.* 0.05% at 47 °C in the ambient gas pressure range 0.1–34 MPa. The experimental method is described and data are provided. These data are used to compute the most effective description of the diffusion process by invoking a number of different diffusion coefficient, $D(\theta)$, characteristics, where θ denotes lapsed time, ambient pressure and local ambient gas concentration within the elastomers. The numerical procedures adopted to perform the fitting of the experimental data with various $D(\theta)$ characteristics are described and the quality of the fit is assessed.

The $D(\theta)$ characteristics chosen have no particular physical basis but follow established empirical precedents. The characteristics of the parameters associated with the various $D(\theta)$ functions generally indicate that as the gas is embibed with progressively increasing ambient pressures the diffusion coefficient increases. At high pressures the diffusion is arrested and the coefficient decreases. We have associated the initial increase with gas induced plasticization and the eventual decreases with the effect of the hydrostatic component of the ambient gas pressure. The parameter fitting also indicates that the diffusion is arrested with lapsed time which is

Phil. Trans. R. Soc. Lond. A (1992) **339**, 497–519
Printed in Great Britain

tentatively associated with time dependent volumetric relaxations. These interpretations apart, the data and analyses clearly indicate that the transport is not simply fickian and a relatively complex parametric function to describe the sensitivity of the diffusion coefficient to time, concentration and pressure is necessary for these systems.

1. Introduction

This paper describes the results of an experimental and analytical study of CO_2 gas sorption in two commercial nitrile based elastomers. These materials are commonly used as seals or connectors in high-pressure gas handling equipment. As such these materials are frequently exposed to fluctuating ambient gas pressures and as a consequence suffer irreversible mechanical damage referred to as explosive decompression rupture. A series of internal cracks, often with a well-defined symmetry, are generated within the elastomer. In the most marked cases the cracks form shapes which are of the same type, but of a smaller size than the section of the elastomer which is examined. Invariably, the samples rupture during decompression and not during compression; the inference is that the samples are ruptured, in part at least, by internal stress gradients which develop by concentration gradients that are created as gas desorbs from the sample. When the ambient pressure is reduced the sample also suffers an overall hydrostatic tension as the pneumatic stress is reduced as well as the inevitable modest thermal shock associated with the adiabatic nature of the decompression. Elsewhere, Briscoe & Liatsis (1992) have argued that the crack initiation is induced by hydrostatic tensile stresses developed within the elastomer as a result of the combined contributions from these two sources; the overall triaxial tensile stress that is imposed by the external ambient and a quasi triaxial stress that is a result of the evolving gas concentration gradients.

The study of this problem has led us to consider means of obtaining an accurate estimation of the ambient pressure and naturally the concentration dependence of the diffusion properties of typical elastomers at elevated pressures. The nature of the decompression or desorption process cannot be addressed directly since the process induces elastomer rupture. This paper describes how the corresponding adsorption data may be obtained and subsequently analysed to produce expressions for the diffusion coefficient as a function of the prevailing ambient conditions. Certain special experimental and analytical techniques have been developed for this purpose and they are described. They are adaptations and extensions of established methods and as such demonstrate the potential for characterizing diffusion processes under rather severe ambient conditions.

The data provided in the paper indicate that the diffusion coefficient is a rather complex function of the prevailing pressure; the process is highly non-fickian. The trends in the data are, however, reasonable when judged in terms of the known diffusion properties of gases in polymers. That is if we accept the notion that the gas pressure may induce a volumetric compression (hydrostatic stress) on the elastomer while the gas is sorbed into the sample. In fact, numerous experimental studies on the density of elastomers as a function of ambient gas pressure do suggest that this is the case.

The paper is presented in two main parts. The first is a description of the experimental method which is essentially the use of a mass sorption technique to

PHILOSOPHICAL TRANSACTIONS OF THE ROYAL SOCIETY A MATHEMATICAL, PHYSICAL & ENGINEERING SCIENCES

follow the sorption as a function of time. The second part of the paper describes how the necessary diffusion coefficient data were obtained. The significance of the results is described in the conclusions of the paper.

2. Materials and equipment

The time dependent gas sorption measurements with CO_2 gas have been carried out in the pressure range 0.1–34 MPa at the temperature of 47 °C. The diffusion characteristics of carbon dioxide in nitrile rubbers with different degrees of compoundings have been evaluated from these data. The nitrile rubbers were commercial elastomers supplied by BP Chemicals. Their compounding varied in the type of rubber, in the type and content of filler and in the cure system. They were studied in the form of rectangular blocks of approximate dimensions 28 mm × 8 mm × 8 mm. The samples were fabricated from the uncured material which was preheated in an air oven at 100 °C for 40 min. Then they were placed in specially made preheated moulds at 153 °C. A temperature controlled hydraulic press was then used for compressing the samples at a pressure of 50 tons on an 8 in. (approx. 20 cm) diameter ram (16 MPa) for 30 min. The rubbers were black in colour because of the inclusion of carbon filters. The physical and mechanical properties of the two nitrile elastomers studied were summarized in table 1. A digest of their composition and the method of preparation is also given there. The two samples were of similar organic composition but varied in the type and amounts of inorganic filler present. Both were nitrile-butadiene–acrylonitrile (28%) copolymers with the same cure system (sulphur-donor with accelerators). Sample A had a 'low', and entirely carbon based, filler content. Sample B contained a lesser fraction of the same carbon but combined with a comparable quantity of a magnesium carbonate; in the context of rubber technology this is regarded as a 'medium' filler content. The carbon dioxide gas used had a nominal purity of 99.5% and was supplied by B.O.C.

The high-pressure system used for these studies consisted basically of a double capped pressure vessel housed in a fluid heat exchanger and an air driven gas booster of a compression ratio of 85:1 capable of pumping up to 55 MPa. An important feature of this system was its ability to maintain a certain pressure and compensate for small leaks and thermal fluctuations. Thus, the long-term pressure stability of the high-pressure system was better than 0.5 MPa. The temperature of the fluid heat exchanger surrounding the pressure vessel was controlled by a platinum resistance thermometer within ± 0.2 °C. A detailed description of the pressure vessel and pumping arrangements can be found elsewhere (Briscoe & Liatsis 1992).

3. Experimental techniques

The most common method used for determining the diffusion coefficient of gases in polymers involves the use of time dependent mass sorption measurements. Robust mass probes are required for the hostile environments used in the current studies and the dynamic nature of such measurements necessitates the use of fast response measuring techniques. A short review of sorption techniques previously used for the quantitative measurement of gaseous solubility in organic polymers is given elsewhere (Briscoe & Mahgerefteh 1984) along with their limitations. The vibrating beam technique described there for mass sorption measurements (Briscoe & Mahgerefteh 1984) meets these requirements and, after certain modifications, has been adopted for the current studies.

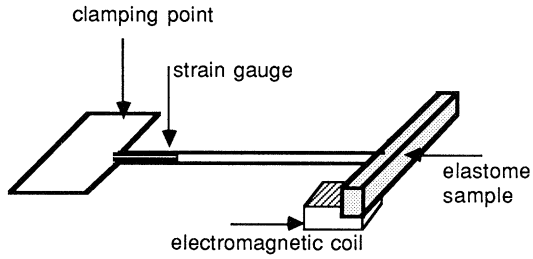

Figure 1. A schematic representation of the vibrating beam probe designed for monitoring high-pressure gas sorption in elastomers.

Table 1. *Physical and mechanical properties of the two nitrile elastomers*

(These are conventional nitrile butadiene copolymer rubbers, which contain *ca.* 28% of acryolonitrile. Each contains a variety of additives, processing aids, plasticizers and antioxidants and the same weight fraction of the base polymer. The cure system is a conventional vulcanization involving a sulphur donor with various accelerators. Both also contained (as a mass fraction of the polymer) a semi-reinforcing black (SRFN762); a fine carbon particle: Sample A, 40 parts; Sample B, 55 parts. In addition, Sample A contained 36.7 parts of magnesium carbonate (talc). Materials supplied by BP Chemicals and preparation involved hot isostatic pressing at 180 °C.)

nitrile elastomer	elastomer density/(kg m^{-3})	tensile strength/MPa	Young's modulus, E/MPa	bulk modulus, B/MPa
A	1328.4	38.8	8.8	3574
B	1187.7	41.3	11.1	2164

The vibrating beam mass detector technique measures the first harmonic resonant frequency of a slender cantilever with an elastomeric sample attached to its free end (figure 1). The resonant frequency changes as the mass of the sample varies during sorption. Monitoring the frequency following a rapid increase in the pressure of the surrounding gas provides the necessary data for obtaining the sorption curves respectively (mass uptake with time). The vibrating beam was made of a special high-carbon magnetic steel (NiSpan-C) of 1 mm thickness and the other dimensions were typically 25 mm × 2 mm. This type of steel has the peculiar merit of producing vibrating reeds whose natural frequency is not very sensitive to the ambient temperature. The beam was excited and driven into resonance by an electromagnetic coil. The resonant frequency at ambient conditions were typically 138 Hz. A strain gauge was bonded onto the beam and the frequency and the amplitude of its vibrations could thus be monitored. The frequency was measured by a Philips PM 6671 high resolution timer/counter 120 MHz at a sampling rate of 10 measurements per second. The amplitude of the oscillations was typically 1 mm and it was sensed by a Keithley 195A digital multimeter. The output signal of the strain gauge was amplified, first by a preamplifier and then by a power amplifier, and fed back to the electromagnetic coil forming a 'closed loop' activating system. In this mode of operation the system was able to tune into the resonant frequency accurately and also rapidly enough (in less than 1 s) to follow the transient responses of the sorption process. One of the recent improvements of the technique was the ability to operate at a constant strain gauge pick-up/output drive coil signal ratio. This was achieved by using a custom built variable-gain strain gauge signal preamplifier. This modification was necessary as the resonance behaviour of these beams is sensitive to the amplitude of their oscillations. The amplitude of the oscillations is sufficiently

sensitive to the ambient gas pressure to warrant such a control of the vibrational amplitude via the adjustment of the nett gain of the pre and power amplifiers. The stability of the vibrating beam probe, in terms of period of oscillations at resonance, was better than 1 μs in 5000 μs. This corresponds, as it is shown in Appendix A, to a mass resolution of 1 mg in a total sample mass of *ca.* 2 g (0.05% mass resolution). In practice, a correction must be applied to account for the entrained gas mass which also induces a frequency change. This correction is obtained by performing a calibration experiment using an inert aluminium specimen of geometry similar to that of the elastomeric sample (Briscoe *et al.* 1986).

A first-order theory of vibrating beams is presented in Appendix A. The method adopted to enable the conversion of the observed changes in the period of oscillations to the mass changes is also explained there. In summary, the mass of the sorbed gas in the elastomer at any time t, $\Delta m(t)$, induced as a result of a pressure step in the ambient at $t = 0$ (P_1 to P_2) is

$$\Delta m(t) = (M_{\mathrm{el}}^{(2)} - M_{\mathrm{el}}^{(1)}) - (M_{\mathrm{Al}}^{(2)} - M_{\mathrm{Al}}^{(1)}), \tag{1}$$

where M denotes apparent masses, the superscripts 1 and 2 denote the pressure conditions P_1 and P_2 respectively, and the subscripts el and Al denote the elastomeric and the inert aluminium samples respectively.

The behaviour of the vibrating beam is strongly related to the value of the ratio of the rest mass attached at the free end to the mass of the reed. The value of this ratio for the beams used in this study was chosen (*ca.* 3) so that the optimum performance was ensured. This procedure is also described in detail in the Appendix A. Consequently, the inert specimen must have the same rest mass as the elastomer specimens so that the inert and the sorbing specimens operate in the same range of the above ratio.

The area of the face of the sample perpendicular to the direction of motion must be kept constant in addition. Otherwise, the entrained mass produced will not be consistent among the various specimens. The area of the face, normal to the direction of motion, is the major geometric factor that controls the magnitude of the entrained mass. Since the aluminium density is about twice the density of the elastomer, the thickness of the elastomer specimens had to be about double the thickness of the reference aluminium specimens. If the area of the side face of the specimen changes substantially, due to sample dilation or contraction, then a second correction must be applied (Briscoe *et al.* 1990). This correction accounts for the observed frequency change due to the increase in the entrained ambient gas mass. One possible reason for such a change in the physical dimensions of the samples could be the sorptive dilation of these elastomeric specimens under high pressure CO_2 gas. The gas sorption into the elastomer often produces a considerable volumetric dilation. However, this is not the case for the systems studied here. The induced volumetric changes have been measured (Briscoe & Zakaria 1990, 1991) and it was found that these changes were not significant enough to justify such a correction. The time for equilibration was often long (4–5 h) and the determination of the equilibrium mass sorption, M_∞, at a particular pressure introduces potentially serious errors. These errors were minimized by plotting the mass data against the inverse of time and using the intercept (for $1/t \to 0$ or $t \to \infty$) as the equilibrium mass values; this is a simple intuitive expedient with no theoretical basis.

Early experiments using nitrogen gas at pressures up to 50 MPa at room temperature indicated that the transport rates for this system were too rapid to be

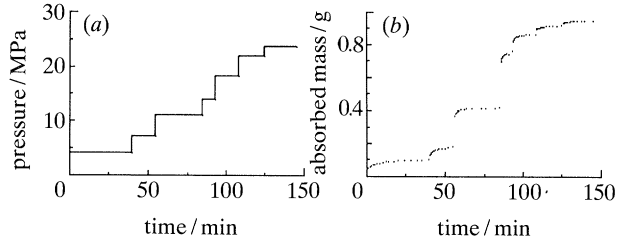

Figure 2. The induced successive pressure increments as a function of time and the corresponding measured mass increase of an elastomeric sample.

followed currently by the instrumentation we have developed. However, the diffusion of carbon dioxide is much slower, permitting the satisfactory recording of transient measurements. Rapid pressure changes were still necessary to ensure that the early time mass measurements were obtained under isobaric conditions. A large intermediate pressure vessel, connected in series with the main pressure vessel containing the sample when brought to a higher pressure, generated a rapid (nearly step function) pressure change. Although these large pressure steps produced pronounced changes in frequency it was found that the accompanying adiabatic effects undermined the value of these data. It was, therefore, found necessary to use rather small incremental pressure changes (3 MPa) in conjunction with fast electronic data collection procedures. The data acquisition system was based on a Comcen PC/XT compatible personal computer equipped with an IEEE 488 interface card and an analog to digital 8 channel card (U-Microcomputers). The measured signals included the pressure, the temperature, the period and the amplitude of vibrations. The developed software allowed automatic acquisition of a full set of measurements every 2 s.

Desorption data were obtained by reducing the pressure in small rapid steps. However, the pressure and temperature fluctuations after each step were too significant to neglect and finally during the last recorded pressure step the sample suffered extensive internal ruptures during depressurization known as 'explosive decompression' failure (Briscoe & Liatsis 1992). The geometry changed dramatically due to swelling and blistering and the probe failed to operate satisfactorily. The use of small pressure steps seems to be the solution to this problem, but the explosive decompression damage of the sample still occurred.

The study reported here is thus confined entirely to the sequential adsorption of gas.

4. Experimental results

As an example of the technique we will describe data on the sorption of CO_2 into a nitrile rubber at 47 °C. A rectangular specimen (28 mm × 8 mm × 8 mm, 2.4724 g) was attached to the vibrating beam probe and the CO_2 mass uptake was followed as a function of time after seven successive pressure increments. Figure 2*a* is a pictorial description of the sequence of these pressure steps as sensed by the ambient pressure transducer. Transient measurements of the period of oscillations at resonance as a function of time were taken in the range of 0.1–25 MPa at 47 °C. As was mentioned earlier, following a pressure increase the ambient pressure and the temperature fluctuated and the resulting effect on the measurements in the early parts of each step was too significant to neglect. Therefore, the validity of the measurements in the first minute of each step is questionable and the corresponding data are not reported.

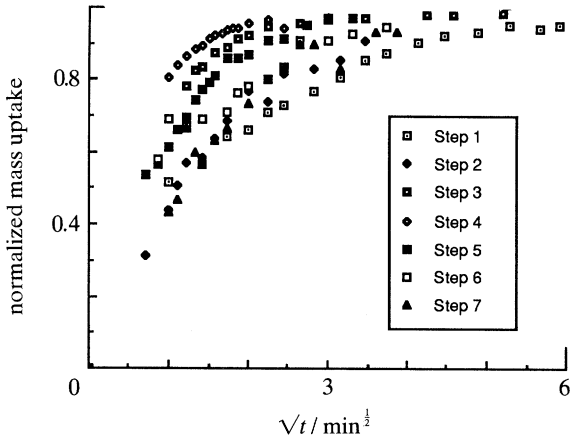

Figure 3. Carbon dioxide mass uptake curves against the square root of time for nitrile elastomer *A* at 47 °C after the seven successive pressure increments depicted in figure 2.

A comparison of figure 2*a*, *b* shows that the equilibrium mass sorption is not a linear function of the ambient pressure, or indeed, the ambient gas density. The adsorption isotherm is, in fact, sigmoidal in shape with a pronounced increase in the sorbed mass between 10 and 20 MPa; in this region the CO_2 enters the supercritical phase.

The obtained data were converted to sorbed gas mass data as a function of time according to the theory of vibrating beams presented in §3 and in Appendix A. The correction for the entrained mass contribution was, of course, taken into account. The transient data, in terms of period of oscillations for a typical pressure step, is presented in Appendix A along with the corresponding calibration line. The subsequent corresponding increase in the mass of the sample during the seven successive pressure steps are also plotted against time in figure 2*b*. The equilibrium mass sorption, M_∞, at a particular pressure was determined by extrapolating to infinite time as described earlier. The cumulative mass sorption at equilibrium is shown in Appendix B as a function of the ambient gas density. The calibration curve is also included. The mass sorbed at any time $M(t)$ during each pressure step, normalized by the total mass sorbed at the end of the step $M(\infty)$, is plotted against the square root of time, $t^{\frac{1}{2}}$ in figure 3. The analysis of these data will be presented in the next three sections of this paper.

5. Preliminary analysis

The diffusion coefficient can be most readily determined from the slope of the mass sorption curves at the early sorption times. Unfortunately, these data were not accessible. The diffusion coefficients were, therefore, determined by considering the whole curves. This was done by comparing the experimentally measured mass curves with the theoretical ones obtained from the solution of Fick's second law of diffusion for concentration dependent and independent D. In later parts of the paper the influence of pressure and time upon D is introduced. In the analysis to follow, the rectangular sample was approximated by a cylinder of such a radius that the two geometries had the same cross-sectional area:

$$\pi a^2 = l^2 \Rightarrow a = 4.5 \times 10^{-3} \text{ m}.$$

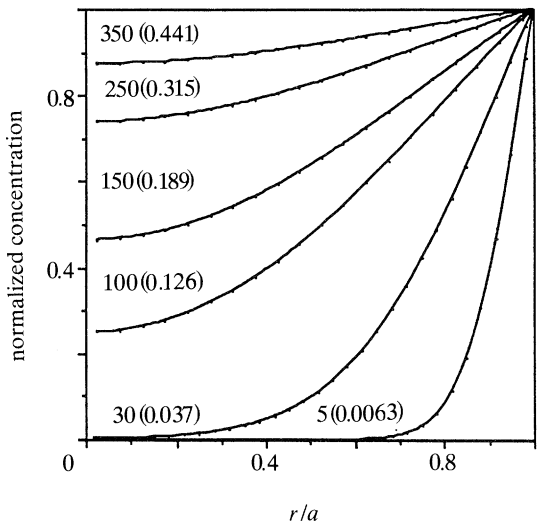

Figure 4. Theoretical concentration profiles at various times t during diffusion in a cylinder of radius a with a constant diffusion coefficient D. The initial concentration C_0 is uniform throughout the cylinder and the surface concentration C_s is maintained constant. Numbers on curves are values of the time in seconds, and in brackets the dimensionless parameter Dt/a^2 (Crank 1975, p. 74).

The non-steady-state diffusion equation for a cylindrical geometry, where r is the radial coordinate, is

$$\frac{\partial C}{\partial t} = \frac{1}{r}\frac{\partial}{\partial r}\left(rD\frac{\partial C}{\partial r}\right). \tag{2}$$

For the case of a constant diffusion coefficient D, if the concentration is initially uniform (time, $t = 0$) throughout the radius of a cylinder, C_0, and the surface concentration, C_s, is maintained constant:

$$\left.\begin{aligned} C &= C_0, & 0 \leqslant r \leqslant a, \quad t &= 0, \\ C &= C_s, & r &= a, \qquad t > 0, \\ \text{and because of the cylindrical axial symmetry:} & & & \\ \partial C/\partial r &= 0, & r &= 0, \qquad t \geqslant 0, \end{aligned}\right\} \tag{3}$$

where a is the cylinder radius, then the solution of equation (2) is given by Crank (1975, p. 73):

$$c = \frac{C - C_0}{C_s - C_0} = 1 - 2\sum_{n=1}^{\infty}\frac{\exp(-Dtb_n/a^2)\,J_0(rb_n/a)}{b_n\,J_1(b_n)}, \tag{4}$$

where J_0 and J_1 are the Bessel functions of the first kind of zero and first order respectively and the b_ns are roots of $J_0(b_n) = 0$. The left-hand side of equation (4) is a normalized expression of the concentration. It ranges from 0 to 1 and in the rest of this paper it will be denoted by c.

Equation (4) gives the normalized concentration c as a function of r/a and these concentration profiles are plotted in figure 4 (Crank 1975, p. 74) with the dimensionless group Dt/a^2 as the operating parameter.

The mass uptake M_t at any time t may be obtained by integrating these concentration profiles, neglecting end effects;

$$\text{mass uptake} = \text{volume} \times \text{concentration}, \tag{5}$$

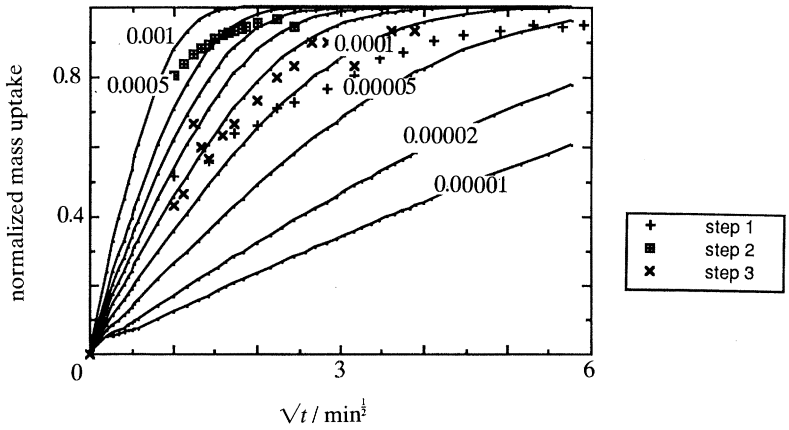

Figure 5. Theoretical mass uptake curves (solid lines) against the square root of time for diffusion in a cylinder of radius 4.5 mm with constant D. The numbers on the curves are values of D. Selected experimental data of figure 3 are repeated here: low, middle and high pressure (steps 1, 4 and 7).

or in terms of the above solution, for a cylinder of height, h,

$$M_t = (h)\int_0^a 2\pi r c(t, r/a)\,\mathrm{d}r, \tag{6}$$

$$M_t = (h)\,2\pi a^2 \int_0^1 \frac{r}{a} c(t, r/a)\,\mathrm{d}(r/a). \tag{7}$$

At equilibrium, reached after infinite time, the dimensionless concentration is 1 and the mass uptake is

$$M_\infty = (h)\,\pi a^2. \tag{8}$$

Hence, the normalized mass uptake is given by

$$\frac{M_t}{M_\infty} = 2\int_0^1 \frac{r}{a} c(t, r/a)\,\mathrm{d}(r/a) \tag{9}$$

and for the constant D case (Crank 1975, p. 73)

$$\frac{M_t}{M_\infty} = 1 - \sum_{n=1}^{\infty} \frac{4}{b_n^2} \exp\left(-Dtb_n^2/a^2\right). \tag{10}$$

Figure 5 shows the above expression plotted against the square root of time for various values of D and for $a = 4.5 \times 10^{-3}$ m (solid lines). Values of b_n were taken from tables (Kreyszig 1979) and it was found that calculations beyond the ninth term of the Bessel functions did not improve the accuracy of the result.

Examination of the experimentally obtained mass curves presented in figure 3 shows that M_t/M_∞ against $t^{\frac{1}{2}}$ for these data are different for each pressure step. Since a normalized y axis is used all curves should superimpose onto one single master curve for simple fickian diffusion. The fact that the curves do not coincide indicates that the diffusion coefficient varies with the ambient pressure and concentration and possibly the time. The trend in the coefficient may be deduced by assuming that the coefficient is constant during each pressure step. Initially, it increases in the first pressure steps, reaches a maximum and decreases in the last steps. For convenience

Table 2. *The assessed expressions for a concentration, pressure and time dependent diffusion coefficient*

case	
1	D_0
2	$D_0 \exp(\alpha C)$
3	$D_0 \exp(\alpha C + \beta C^2)$
4	$D_0 \exp(\alpha C + \beta C^2 + \gamma C^3)$
5	$D_0 \exp(\alpha C) \exp(\beta P)$
6	$D_0 \exp(\alpha C) \exp(\beta P + \gamma P^2)$
7	$D_0 \exp(\alpha C + \beta C^2) \exp(\gamma P + \delta P^2)$
8	$D_0 \exp[\alpha C \cdot (1 - \exp(-t/\tau_1))] \exp[\beta P(1 - \exp(-t/\tau_2))]$
9	$D_0 \exp[(\alpha C + \beta C^2)(1 - \exp(-t/\tau_1))] \exp[\gamma P \cdot (1 - \exp(-t/\tau_2))]$
10	$D_0 \exp[(\alpha C + \beta C^2)[\gamma \exp(-t/\tau) + 1 - \gamma]]$
11	$D_0[\gamma \exp(-t/\tau) + 1 - \gamma] \exp(\alpha C + \beta C^2)$
12	$D_0[\gamma \exp(-t/\tau) + 1 - \gamma] \exp(\alpha C + \beta C^2) \exp(\delta P)$

in this comparison selected experimental data of figure 3 are reproduced against the theoretical curves in figure 5. In particular, steps 1, 4 and 7, which are the low, middle and high pressure steps, are replotted. A first-order visual comparison shows almost an order-of-magnitude difference between the minimum and maximum values. This variation of D with the ambient gas pressure (or concentration or time) shows clearly two trends: at low pressures the dependence is positive and at higher pressures it is negative. A diffusion coefficient increasing with concentration is a very common observation and, in particular, for the diffusion of liquid hydrocarbons in polymers (Prager & Long 1951). The same trend was observed for the diffusion of CO_2 in PET (Koros *et al.* 1977). It is suggested that the gas plasticizes the polymer and, therefore, increasing gas concentration promotes the diffusion of the gas through the molecular chains. At higher pressures the pressure dependence of D is consistent with the anticipated free volume reduction (Rennie & Tabor 1980): the free volume of the elastomer decreases with increasing hydrostatic pressure and, therefore, D is a decreasing function of pressure. Furthermore, a casual comparison of the experimental and the theoretical constant D mass curves reveals that their forms are very different. This implies that the diffusion coefficient is a strong function of the gas pressure and the concentration even *during* each pressure step. The analysis presented in the next section will consider a pressure and concentration dependent diffusion process. For completeness a time dependence is also included. Various forms of these dependences will be assessed and table 2 lists these expressions.

The first expression is the fickian case where the diffusion coefficient is taken to be a constant and equal to D_0. The second case involves an exponential dependence of D on concentration. The third and the fourth cases are exponential expressions of the concentration in the second and third power respectively. The fifth case involves exponential dependences on both the concentration and the pressure. The sixth and seventh cases are similar expressions involving higher powers of the pressure and the concentration. The last five expressions include a time-dependent term. In expressions (8)–(12) time is included as an exponentially decaying term which operates on both the pressure and the concentration. It effectively retards the effect of the pressure and the concentration on the diffusion coefficient.

The set of the fitting parameters D_0, α, β, γ, δ, τ_1 and τ_2 that appear in the expressions given in table 2 will be referred to as general parameters, θ. Hence, the

PHILOSOPHICAL TRANSACTIONS OF THE ROYAL SOCIETY A MATHEMATICAL, PHYSICAL & ENGINEERING SCIENCES

diffusion coefficient can be considered to depend on the concentration, the pressure, the time or on a set of parameters θ. In terms of the above notation:

$$D = D(C, P, t) = D(\theta). \tag{11}$$

It should be noted that D depends on the absolute value of concentration C and not on the normalized concentration c. The latter always ranges from 0 to 1 and following the introduction of a pressure increment the relation between $C(t_f)$ and $c(t_f)$ is given by

$$C = C_i + c(C_f - C_i), \tag{12}$$

and C_i and C_f refer to the initial and final gas concentrates in weight fraction units.

6. Data processing strategy

The basic requirement is to produce a means of generating mass sorption data on the basis of a diffusion coefficient whose numerical values are functions of chosen variables; a number of interrelations of this type are given in table 2. For certain, usually simple, non-constant diffusion coefficients analytical solutions are available (Crank 1975). The utilization of the expressions for the diffusion coefficient given in table 2 require numerical solutions. The principle is straightforward, and is detailed below, but the implementation of such procedures requires rather sophisticated numerical methods if accurate solutions are to be obtained in an efficient manner. The essential feature is the adoption of a criterion to facilitate the comparison of prediction and experiment; we have followed the well established route of minimizing the sum of the squares of the residuals. The various numerical procedures seek to do this in the most efficient and accurate way. It should be borne in mind that many of the expressions for the diffusion coefficient, chosen to some extent on an arbitrary basis, produce ill-conditioned solutions where the sum of the squares of the residuals is not a profound assessment of the quality of the fitting process. In such cases, solutions do not readily converge which necessitates the resort to the methods to be described.

The specific aim described here is to determine those values of the parameters θ (equation (11)) occurring in each of the relationships given in table 2 by fitting the predicted mass uptake curves to the experimental data. A test of the quality of the fitting is required, one was introduced earlier, and a further type of test is described later. The parametric evaluation has been achieved by solving equation (2) with the diffusion coefficient relations given in table 2 in combination with equation (9). These predictions have then been compared with the experimental data. The procedure used to carry out the fitting was a nonlinear least squares (NLSQ) method; that is, one seeks to minimize the error between the predicted and the measured curves; the sum of the squares of the residuals. A number of parameters are defined as follows. K is the number of pressure steps, K_s is the number of experimental points at the sth pressure step, $M_{s,j}$ and $\bar{M}_{s,j}$ the predicted and experimental values of the normalized mass uptakes at time $t_{s,j}$ respectively, where $t_{s,j}$ is the jth experimental measurement at the sth pressure step. The objective function $S(\theta)$ is defined as the weighted sum of squares of the errors

$$S(\theta) = \sum_{s=1}^{k} \sum_{j=1}^{k_s} \phi_{s,j}^2(\theta), \tag{13}$$

$$\phi_{s,j}(\theta) = w_{s,j}(M_{s,j} - \bar{M}_{s,j}), \tag{14}$$

where the weights $w_{s,j}$ may be used to reflect the relative accuracy of each experimental point. Such weighting was not adopted in this study. The relative magnitudes of $S(\theta)$ provides a measure of the quality of the fitting of the data.

A precondition for the parameter estimation is the ability to calculate the value of the objective function $S(\theta)$ for any given value of θ within the feasible region. In this case, it means that it is necessary to solve the diffusion equation (2) for the concentration profile and then calculate the mass uptake from equation (9). Since analytical solutions of the diffusion equation are only available for the case when D is not a function of the concentration, i.e. constant, it is necessary to use a numerical method that gives the concentration profile as a function of time. The partial differential equation (PDE) (2) has been solved by the method of lines (MOL) which is often used to solving parabolic, time-dependent PDEs like (2) (Ames 1977). The procedure involves the discretization of the spatial variable r and the approximation of the partial derivatives with respect to r by finite differences. In this way, the PDE and its boundary conditions are transformed to a set of ordinary differential equations (ODEs) which are then solved by a method suitable for that problem. Two important advantages of the MOL are that it is computationally efficient and requires a relatively little amount of coding work since the user has only to be concerned with the discretization of the spatial domain (Brenan *et al.* 1989). Because the ODEs obtained by the MOL may be 'stiff', an implicit integration method is utilized for their solution. Consider now a uniform partition of the interval $[0, 1]$ into N subintervals and let $r_i = i/N$, $i = 0, \ldots, N$. The MOL calculates the concentration profile at time t in the discrete points r_i, $c_i(t)$ by solving a set of ODEs of the following form:

$$X'(t) = F(X(t), \theta, t), \quad C(t = 0) = C_0, \tag{15}$$

where $X'(t) = \mathrm{d}X(t)/\mathrm{d}t$ and $X(t) = [c_0(t), \ldots, c_N(t)]$. Having computed $C(t)$, the normalized mass uptake is then calculated from equation (9) by means of an integration formula (for instance, Simpson's rule) as below:

$$M(t) = \sum_{i=0}^{N} \gamma_i r_i c_i(t), \tag{16}$$

where the weights γ_i are formula dependent. Hence, to calculate the terms of the objective function corresponding to the sth pressure step, it is sufficient to compute the numerical solution of equation (15) at time $t_{s,j}$, $j = 1, \ldots, K_s$, and then use equation (16) to compute the associated mass uptake. Repeating this process for all pressure steps finally yields the value of the objective function. The derivation of the ODEs (equation (16)) and issues associated with their solution are discussed further in Appendix C.

It was decided in this study to utilize a NLSQ algorithm which requires not only the values of $\phi_{s,j}(\theta)$ but also the gradients of $\phi_{s,j}(\theta)$ with respect to θ, $\partial\phi_{s,j}/\partial\theta$, due to the robustness and efficiency characteristics of such algorithms (Bard 1974, p. 117). Without the inclusion of these gradients, which essentially reflect the sensitivity of the parameter, the solutions invariably did not converge. These gradients are computed by integrating linearized forms of the equation (15), known as the *sensitivity equations*; their integration can be carried out in tandem with the integration of ODEs (equation (15)) exploiting the properties of the numerical scheme used to solve them. The derivation of the sensitivity equations and their efficient integration are also discussed in Appendix C.

The final, and most telling, assessment of the quality of the fitting was carried out

Table 3. *The computed optimal values of the parameters appearing in the expressions of table 2 for carbon dioxide sorption in nitrile elastomer A (figure 3)*

(The units of α, β, γ, δ are such as to produce the necessary dimensional quantities. Concentration units gram/gram, pressure units megaPascal.)

case	$D_0/(10^{-8}\ \mathrm{m^2\ s^{-1}})$	α	β	γ	δ	τ_1/s	τ_2/s	S
1	2.55	—	—	—	—	—	—	1.3502
2	1.78	0.01464	—	—	—	—	—	1.261
3	0.44	0.2389	−0.005365	—	—	—	—	0.3144
4	0.655	0.12257	0.0015817	−0.000111	—	—	—	0.28025
5	3.88	0.12231	−0.229332	—	—	—	—	0.882
6	0.237	0.02287	0.3589703	−0.013551	—	—	—	0.37045
7	0.693	0.28768	−0.005714	−0.133212	0.0023214	—	—	0.2977
8	3.40	0.19023	−0.388547	—	—	67.35102	82.4332	0.6674
9	0.60	0.21783	−0.004493	−0.069928	—	0.0008496	97.7112	0.17005
10	0.43	0.25969	−0.005904	1	—	0.007838	—	0.30143
11	1.05	0.18902	−0.004269	0.713415	—	31.78289	—	0.14623
12	0.139	0.19951	−0.003748	0.7360178	−0.02456	142.6425	—	0.11933

by inspection of the $S(\theta)$ values, equation (13), and by computing and plotting the *residuals*, R_s, as a function of lapse time for each dataset. The residuals are defined as

$$R_s = C_\mathrm{e} - C_\mathrm{p},$$

where C_e and C_p are the experimental and predicted values of the normalized mass concentrations respectively.

7. Results of the parameter estimation procedure

The expressions for the diffusion coefficient listed in table 2 were evaluated against the experimental data. The time invariant D cases are considered first. The parameters θ were estimated according to the methodology described in the previous section. Table 3 summarizes the results of this optimization procedure and lists the computed values of these parameters for the twelve special cases of table 2. These estimates of the parameters minimize the sum of the squares of the residuals, S, which is also included in table 3. Generally, the value of S decreases as the number of the parameters used increases and the expression becomes more complex. Naturally, such a trend is expected. The inclusion of an exponential concentration term has the expected effect (case 2). The introduction of the second power of concentration in the argument of the exponential term improves dramatically the accuracy of the predicting model (case 3). The third power term in concentration offers a further but modest improvement (case 4). The specific introduction of the pressure as one of the variables does not lead to any very major improvement (case 5). The accuracy increases only when pressure and concentration terms of higher order are included (cases 6 and 7). In particular, the negative sign of certain terms is responsible for the characteristic trend of the diffusion coefficient with concentration and pressure; it initially increases and later decreases as the concentration and pressure then increases. In case 6 this is restricted to the term in P^2 whereas in case 7 both the C^2 and P terms are negative. The incorporation of the time-dependent terms adds to the accuracy of the model; compare cases 5 and 8. The introduction of a second-order term again proves to be very beneficial (case 9).

The results obtained for the expression shown in table 2 as case 7 are illustrated in figures 6 and 7. The former shows the computed concentration profiles developed

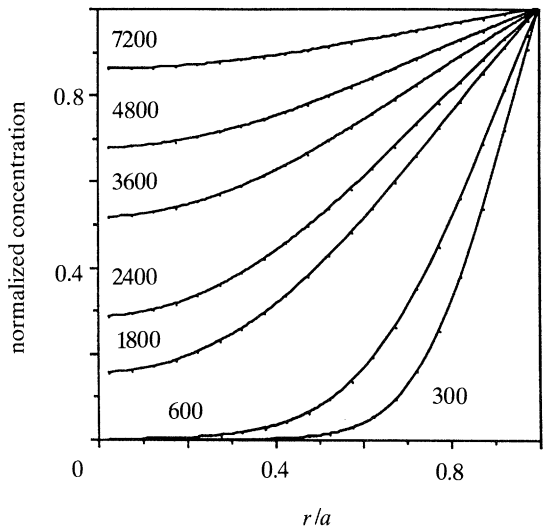

Figure 6. Normalized concentration profiles at various times (in seconds) during diffusion computed for a pressure and concentration dependent diffusion coefficient (case 7 of tables 2 and 3). This figure may be usefully compared with figure 4. The pressure increases from 0.1 MPa to 23.6 MPa while the surface concentration C_s is maintained constant at 0.385 g/g.

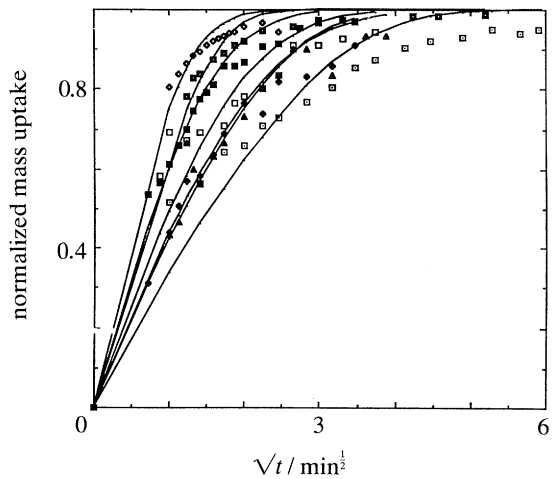

Figure 7. Mass uptake curves fitted to the experimental data of figure 3. These curves were calculated for a concentration and pressure dependent diffusion coefficient (case 7 of tables 2 and 3).

at various times during diffusion into a cylindrical specimen, where the diffusion coefficient depends on the pressure and concentration and follows the above expression. It is interesting to compare these profiles with the ones corresponding to fickian diffusion presented in figure 4. The pressure and concentration dependent profiles are very different to the fickian ones in their scales but are essentially of the same form. Both show, in certain regions, rather rapid decreases in concentration, at particular time periods. These rapid concentration decreases correspond, it may be argued, to changes in the gas pressure across the specimen. It has been suggested (Briscoe & Liatsis 1992) that these pressure discontinuities are largely responsible for the characteristic, internal and concentric cracks observed during rapid depress-

PHILOSOPHICAL TRANSACTIONS OF THE ROYAL SOCIETY A MATHEMATICAL, PHYSICAL & ENGINEERING SCIENCES

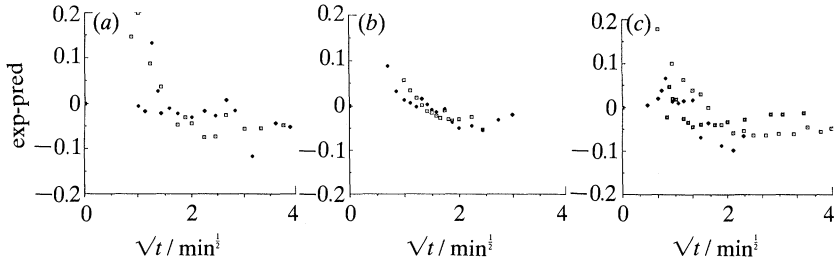

Figure 8. Residual plots for case 7. Evidence of underfitting is apparent. (*a*) ⊡, exp-pred 6; ◆, exp-pred 7. (*b*) ⊡, exp-pred 4; ◆, exp-pred 5. (*c*) ⊡, exp-pred 1; ◆, exp-pred 2; ■, exp-pred 3.

Table 4. *The computed optimal values of the parameters appearing in the expressions of table* 2 *for carbon dioxide sorption in nitrile elastomer* B

case	D_0/(m^2 s^{-1})	α	β	γ	δ	τ_1	τ_2	S
1	3.4×10^{-8}	—	—	—	—	—	—	6.6547
2	1.11×10^{-3}	−0.1807	—	—	—	—	—	2.9423
3	3.04×10^{-12}	0.47848	−0.005314	—	—	—	—	1.163
4	—	—	—	—	—	—	—	0
5	1.99×10^{-9}	0.26182	−0.518164	—	—	—	—	1.9356
6	2.01×10^{-9}	0.2764	−0.571979	0.0006386	—	—	—	1.9339
7	7.09×10^{-15}	0.87146	−0.011466	−0.074053	0.009076	—	—	0.4489
8	5.22×10^{-9}	0.19399	−0.430069	—	—	4.76627	8.87609	1.4807
9	7.37×10^{-15}	0.66676	−0.010916	0.5827737	—	0.029447	0.00025	0.5664

urization of the ambient gas in these types of elastomer. When the external gas pressure is removed, the gas that has already saturated the specimen diffuses out and stress profiles, with characteristics similar to the profile of figure 6 are thought to be formed. These stress gradients are superimposed upon the uniform hydrostatic tensile component generated by the rapid removal of the ambient pneumatic stress. The prediction of the *desorption* profiles from the expressions given in table 2 with the optimized values of the coefficients is relatively straightforward. This facilitates the predictions of the internal stress gradients during decompression.

Figure 7 shows the computed mass uptake curves which are obtained when the diffusion coefficient described by the expression of case 7 is fitted to the experimental data. The values of the parameters used here have been determined by the numerical technique described in the previous section and they are shown in table 3. The agreement between these theoretically predicted mass uptake curves and the experimental data of figure 3 is fair. It appears that this form of the diffusion coefficient predicts successfully not only the basic trends of the diffusion coefficient with increasing gas pressure, i.e. initially increasing and later decreasing, but the shape of the mass uptake curves as well. However, inspection of the residual plot (equation (17)) shown in figure 8 indicates that case 7 is underfitting the experimental data. At short times the computed values are underestimating the experimentally observed data. At longer times the situation is reversed.

Table 4 presents the best estimates of the parameters θ for a different elastomer; sample B. In general, the fitting technique has not given results as successful as for the first elastomer. The values of the sum of the squares are higher here. The optimization method failed to estimate the parameters in case 4. However, the same general observations can be made. The introduction of higher order terms of concentration and pressure offers a significant improvement in the accuracy of the

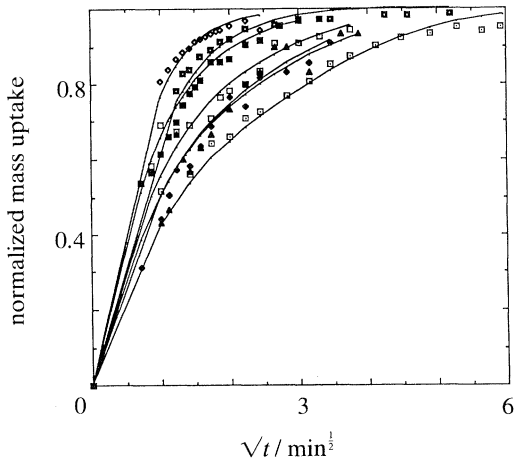

Figure 9. Experimental and calculated mass uptake curves (case 12). Compared with figures 4 and 7 there is an improvement in the correspondence of experimental data and predicted data.

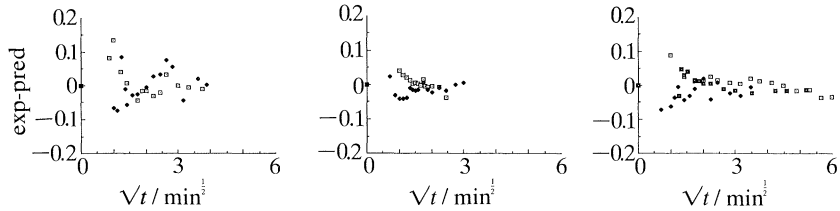

Figure 10. Residual plots for case 12. Less evidence of underfitting is seen compared with figure 8. (Legends as figure 8.)

model. Also the signs of the corresponding coefficients are generally the same; for example the pressure coefficient denoted by β is usually negative for both cases. The function given by equation (7) was found again to underfit the experimental data in a similar way to sample A.

At this stage, rather than include higher terms in C and P, a time variation in D was introduced. The time variable was chosen so that $t = 0$ at the inception of each pressure step. Two cases, 8 and 9, have been applied to both elastomers. Cases 10–12 were evaluated with elastomer A only. The residual sums are reduced by including the time dependence in concentration and in pressure although the improvement is not very dramatic. The residual plots also show that the trend to underfit, evident in figure 8, is still apparent. The mathematical characteristic of cases 8 and 9 is to under weight the short-time predicted values of D compared with the long-time values where the converse is noted. Cases 10–12 introduce the time variable in such a manner that the short time computed values of D have a natural tendency to be greater in magnitude. Expression (12) provides the smallest sum of the square of the residuals and also the most satisfactory residual plots. Figure 9 shows the comparison of experiment and prediction and figure 10 the corresponding residual plots.

8. Discussion of results

The experimental and analytical methods described clearly indicate that a fickian diffusion coefficient cannot satisfactorily account for the data obtained: case 1 (table 2) is a very poor description of the variation of the gas sorption with time. An

inspection of figure 5 demonstrates this fact. The inclusion of concentration dependence with progressively higher order terms naturally improves the fit of the data to the chosen expressions. Here we will consider the data in tables 3 and 4. Thus cases 2–4 show improvements as judged by the comparative sizes of the sums of the squares of the residuals. However, cases 3 and 4 (table 2) contain strong negative terms in C^2 and C^3 respectively. In case 4 the expression is efficient but perhaps is not a good reflection of the physics involved; as C increases so does the pressure. Intuitively, we have suggested that an increase in pressure will arrest the diffusion process and, hence, decrease D. Cases 5 and 6 explore this possibility by introducing a hydrostatic term directly. Case 5 is economical but not efficient although the signs of the terms are in the correct form. The diffusion coefficient increases with concentration but decreases with pressure. More terms in concentration and pressure mainly preserve the expected signs of the parameters and actually improve the quality of the fit; the residuals decrease in magnitude. Generally in this set case 7 is the most effective for table 3. Case 6 is almost as efficient. These results are broadly consistent with the idea that the CO_2 gas plasticizes the matrix and, hence, increases the diffusion coefficient. At the same time the corresponding increase in the ambient pressure arrests the rate of diffusion. Case 5, which contains only two variables other than D_0 is a fair fit of the data for the second elastomer.

The elementary introduction of two time dependent terms is not very useful in reducing the magnitudes of $S(\theta)$. Obviously, the fit as measured by $S(\theta)$ improves as the terms are introduced. Of much more importance is, however, the result that the time variables produce a much closer correspondence between prediction and experiment as judged by the residual plots; compare figures 8 and 10. The inference is that the magnitude of $S(\theta)$ is not a very good indication of the quality of the fit. The effect of the time variables is essentially to slow the diffusion at long times compared with short times. This may be interpreted as evidence for retardation effects in hydrostatic compression or solvent induced dilation. For example, case 9 is an effective but not the most efficient descriptor. Six terms are now operational in case 9 and the residual sum is small. We may also note that case 8 is not very effective. If the magnitudes of the characteristic terms are significant we may also deduce that the characteristic relaxation times for the pressure and concentration terms are quite short compared with the timescale of the experiment. They are never greater than 2 min and are elsewhere either zero or close to zero minutes; the experimental time is typically 35 min. There are some physical grounds to substantiate the belief in a separate time dependent and the analysis does indicate that the diffusion coefficient has a fairly pronounced time dependence. The residuals reduce in magnitude but the time coefficients are small in their absolute magnitude. It is worth noting at this stage that the computed characteristic times are all of a positive sign. As noted earlier, the time characteristics greatly improve the fits at short times as judged by the residual plots.

Of the various sets of relations examined we may now note the efficiency of case 7 and re-examine the sign and magnitude of the operating constants for pressure and concentration. For both samples we have

$$D = D_0 \exp\left[\alpha C(1-\beta C/\alpha)\right] \exp\left[\gamma P(1-\delta P/\gamma)\right] \tag{17}$$

with $\alpha \approx \beta$ and $\gamma \approx \delta$. The choice of exponential variables was arbitrary and follows established precedents. The main point, however, is that the data and analysis strongly suggest the dual action of the ambient gas; as gas concentration increases

PHILOSOPHICAL TRANSACTIONS OF THE ROYAL SOCIETY A MATHEMATICAL, PHYSICAL & ENGINEERING SCIENCES

D increases but by the same token as pressure increases D decreases. This result, coupled with the apparent sensitivity of the transport process to time, are the major deductions to be drawn from these data and their analysis. The physical causes of these effects cannot be resolved on the basis of the present work. However, it is likely that the concentration effects on the diffusion coefficients arise from local variations within the concentration gradients. The hydrostatic term may, to a first order, provide a uniform influence upon the coefficient. In reality, both the concentration and pressure influences are probably time dependent; volume dilations due to plasticization and contraction as a result of hydrostatic stress are most certainly time-dependent phenomena. The time dependence of the diffusion coefficient detected here presumably reflects contributions from both processes.

9. Conclusions

The vibrating beam method is a suitable means of obtaining mass sorption data for certain elastomers at high pressure. The analysis of these data produced a result that strongly suggests that for these elastomers, which are quite typical of many filled elastomeric formulations, the diffusion coefficient follows a form where the coefficient increases with gas concentration but decreases with the associated pneumatic stress. The time dependence of the process is not strong. This result is consistent with the ideas that the gas plasticizes the matrix and, hence, facilitates gas transport. At the same time the associated pneumatic stress compresses the elastomer and arrests the transport. The volumetric relaxations are sufficiently rapid under the chosen conditions to facilitate a rapid molecular readjustment so that no major time dependence is observed in the results. At low ambient pressures the sample dilation is predominant and transport is accelerated. At high pressures, despite the continued sorption, the pneumatic stress becomes predominant. The time characteristic is indicative of a reduction in the diffusion coefficient with lapsed times. In physical terms this may reflect a short time, say a few minutes, volume relaxation induced by the hydrostatic stress or the plasticizing migrating gas species.

Appendix A

According to the theory of vibrating beams clamped at one end and having a rest mass attached at the free end the frequency data (or period) described above can be converted into mass uptake data. For a thin rod of length l, density ρ_s, with Young's modulus E the period of vibration T at resonance is given by

$$T = (2\pi/k)\,(1/z)^2 \sqrt{(\rho_s/E)}, \tag{A 1}$$

where k denotes the radius of gyration of a section of the rod about the axis through its centre of gravity, perpendicular to the plane of motion (Prescott 1924). The variable z satisfies the equation

$$\frac{1+\cosh z \cos z}{\cosh z \sin z - \sinh z \cos z} = Rz, \tag{A 2}$$

where R is the ratio of the rest mass attached at the free end to the mass of the rod. Using these two equations a change in period T can be translated into a change of the ratio R and consequently of the sample mass (Briscoe *et al.* 1986). The period of oscillations T is inversely proportional to the square of the variable z. The latter can

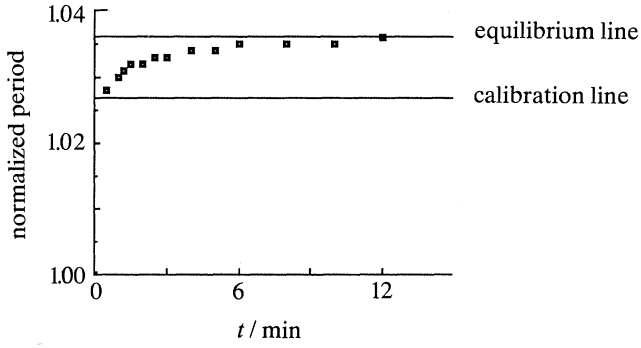

Figure 11. Normalized period (initial period: 7.232 ms) as a function of time for a nitrile elastomer sample following a step function pressure change (step 2 of figure 2).

be determined numerically from equation (A 2) for a given ratio R. Hence, an increase in the period T corresponds to a decrease in the variable z (given from equation (A 1)) which in turn corresponds to an increase in the ratio R calculated numerically from equation (A 2). Such an increase in the ratio R may result from an increase in the mass of the sample.

The increase of the mass of the sample is due to the gas that has diffused into the sample as well as to the entrained gas mass. Therefore, the mass of the sorbed gas in a pressure step (P_1–P_2) is

$$\Delta m = (M_{\mathrm{el}}^{(2)} - M_{\mathrm{Al}}^{(2)}) - (M_{\mathrm{el}}^{(1)} - M_{\mathrm{Al}}^{(1)}). \tag{A 3}$$

The mass of the absorbed gas at any time t in a pressure step (P_1–P_2) is

$$M_1 = \Delta m(t) = (M_{\mathrm{el}}^{(2)}(t) - M_{\mathrm{Al}}^{(2)}) - (M_{\mathrm{el},\infty}^{(1)} - M_{\mathrm{Al}}^{(1)}), \tag{A 4}$$

where infinite time denotes that equilibrium sorption has been reached.

In a pressure step a calibration experiment, as mentioned earlier, is necessary for the evaluation of the entrained gas mass contribution to the observed frequency drop. The fact that the resonant frequencies of the sample and of the inert specimen do not coincide does not cause any difficulty in the sorbed gas mass calculations as only relative frequency changes are required; a trivial rearrangement of equation (A 3) shows that only terms of relative change are involved:

$$\Delta m = (M_{\mathrm{el}}^{(2)} - M_{\mathrm{el}}^{(1)}) - (M_{\mathrm{Al}}^{(2)} - M_{\mathrm{Al}}^{(1)}). \tag{A 5}$$

Appendix B

Specimen raw data are presented here. The transient measurements of the period of oscillations at resonance taken for step 2 are shown in figure 11. The readings of the period have been normalized by the value taken at equilibrium at the end of the previous step. Hence, the first point is unity and the last one corresponds to equilibrium conditions achieved at the end of this step. The horizontal line, denoted as calibration line, corresponds to the change of the period of oscillations at resonance of the inert aluminium sample from the pressure conditions of step 1, where it is unity, to that of step 2.

Both the elastomer and the aluminium data are then converted to mass data following the analysis presented in Appendix A. Their difference, which is the gas mass uptake, plotted against $\sqrt{t}$ produces one of the mass curves of figure 3.

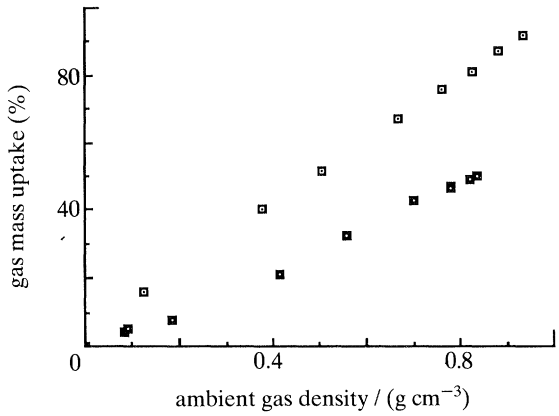

Figure 12. Carbon dioxide mass uptake at equilibrium (grams of gas per 100 g of elastomer) against CO_2 gas density for both the nitrile elastomers at pressures up to 40 MPa at 47 °C. ⊡, nitrile elastomer *A*; ■, nitrile elastomer *B*.

The gas equilibrium sorption of CO_2 in both nitrile rubbers assessed in this paper at 47 °C is presented in figure 12. The data are plotted in terms of percent gas mass uptake against the ambient gas density. The sorption data appears to be proportional to the gas density rather than to the gas pressure. Similar linear relations have been recorded previously for polymers (PTFE) (Briscoe & Mahgerefteh 1984) and silicone elastomers (Briscoe & Zakaria 1990, 1991; Briscoe *et al.* 1986). The high level of CO_2 gas sorption in these rubbers should be pointed out; the value at the maximum pressure exceeds 90% by weight.

Appendix C

The purpose of this appendix is to present in some detail the numerical scheme utilized to solve the PDE equation (2) and also the method by which the gradients $\partial\phi_s/\partial\theta$ are computed.

Consider now the PDE equation (2) with the diffusion coefficient given as

$$D = D(C, \theta, q), \tag{C 1}$$

where q is a set of independent variables the value of which is constant within a pressure step. Partition the interval $[0, 1]$ into N subintervals of equal length, let $h = 1/N$, $r_i = i/N$, $i-0, \ldots, N$. The MOL yields the solution of equation (2) at r_i, $c_i(t)$, by transforming the PDE into a system of ODES. The first and second partial derivatives of c with respect to r at r_i are approximated by the following centred finite differences scheme:

$$\left(\frac{\partial c}{\partial r}\right)_{r_i} = \frac{c_{i+1} - c_{i-1}}{2h}, \quad \left(\frac{\partial^2 c}{\partial r^2}\right)_{r_i} = \frac{c_{i+1} - 2c_i + c_{i-1}}{h^2}, \quad (i = 1, \ldots, N-1), \tag{C 2}$$

while the corresponding scheme of the partial derivative of D is

$$\left(\frac{\partial D}{\partial r}\right)_{r_i} = \frac{D(c_{i+1}, \theta, q) - D(c_{i-1}, \theta, q)}{2h}, \quad (i = 1, \ldots, N-1). \tag{C 3}$$

Application of the above approximations at the points r_i, $i = 1, \ldots, N-1$, yields the following ODEs:

$$c_i' = \frac{c_{i+1}-c_{i-1}}{2h}\frac{D(c_{i+1},\theta,q)-D(c_{i-1},\theta,q)}{2h} + D(c_i,\theta,q)\frac{c_{i+1}-2c_i+c_{i-1}}{h^2} + \frac{D(c_i,\theta,q)}{r_i}\frac{c_{i+1}-c_{i-1}}{2h}, \quad i = 1, \ldots, N-1. \quad (C\,4)$$

The boundary conditions at $r = 1$ yields the equation

$$c_N = 0, \quad (C\,5)$$

while the boundary condition at $r = 0$ is approximated by a non-centred difference scheme

$$\left(\frac{\partial c}{\partial r}\right)_{r_0} = \frac{-c_2+4c_1-3c_0}{h}, \quad (C\,6)$$

which is then used to obtain c_0 as a function of c_1 and c_2

$$c_0 = (4c_1-c_2)/3. \quad (C\,7)$$

Consider now the equations (C 4) for $i = 1, \ldots, N-1$ with c_0 and c_N being substituted from equations (C 7) and (C 5) respectively. These equations constitute a set of $N-1$ differential equations in terms of $N-1$ unknowns, namely $c_1, \ldots, c_{N-1}$. It follows from the initial conditions of the PDE (2) that the initial conditions of the MOL ODEs are $c_i(0) = 0$, $i = 1, N-1$. Given the values of the parameters θ and the variables q, they can be integrated by a numerical method to give $c_1, \ldots, c_{N-1}$ as a function of time, while c_0 and c_N are computed via equations (C 7) and (C 5) respectively. Finally, the predicted mass uptake is calculated by means of an integration formula:

$$M_{s,j} = \sum_{j=1}^{k_1} \gamma_i r_i c_i(t_{s,j}). \quad (C\,8)$$

The derived ODEs are solved by DASSL (Petzold 1983), an automatic code implementing Gear's method (an implicit multistep method) which is suitable for stiff ODEs (Gear 1971). Gear's method computes the solution of ODEs in a stepwise fashion; at each step a set of non-linear equations, henceforth called *corrector equations*, are solved by a Newton-like method. The MOL ODEs have a particular structure because the right hand side of the ith equation (C 4) contains the variables c_{i-1}, c_i and c_{i+1} only. Hence, the corrector equations have a tridiagonal form and, as a result, their solution involves the factorization of a tridiagonal matrix. To improve the efficient performance of DASSL, we provide analytically the jacobian of the corrector equations; the major part of it is the calculation of the partial derivatives of the right-hand side of the ith (equation (C 4)) with respect to the variables c_{i-1}, c_i and c_{i+1}. This task is carried out by differentiation and application of the chain rule.

We turn now to the calculation of the gradients $\partial\phi_{s,j}/\partial\theta$. Clearly, $\phi_{s,j}(\theta)$ is not available in an explicit form and therefore it cannot be differentiated directly to give the desired gradients. Use of a finite differences technique enables the calculation of the gradients; it involves the perturbation in turn of each θ variable and the integration of the ODEs using the perturbed value of θ. Despite its simplicity such an approach may be computationally more expensive and, more importantly, it suffers

from the inaccuracies associated with finite differences techniques. An alternative approach adopted here is that of *sensitivity analysis* for the ODEs (equation (C 4)). To shorten the notation, the ODEs (equation (C 4)) are now written as

$$Y'(t) = f(Y(t), \theta, t), \tag{C 9}$$

where $Y(t) = [c_1(t), \ldots, c_{N-1}(t)]$. Differentiation of the above equation with respect to θ together with application of the chain rule gives

$$\frac{\mathrm{d}}{\mathrm{d}t}\left(\frac{\partial Y}{\partial \theta}\right) = \left(\frac{\partial F}{\partial Y}\right)\left(\frac{\partial Y}{\partial \theta}\right) + \left(\frac{\partial f}{\partial \theta}\right), \tag{C 10}$$

while the corresponding initial conditions are:

$$(\partial Y/\partial \theta)_{t=0} = 0. \tag{C 11}$$

The above linear ODEs are the *sensitivity equations* for the ODEs (equation (C 9)). The variables $\partial Y/\partial \theta$ are called *sensitivity coefficients* and their value is a measure of how sensitive the variables $Y(t)$, i.e. $c_1(t), \ldots, c_{N-1}(t)$ are to variations of the parameters θ. Given the solution of equation (C 9), the sensitivity coefficients are computed by integrating the equations (C 10). Once the sensitivity coefficients are available, the gradients $\partial \phi_{sj}/\partial \theta$ are obtained by the following relation:

$$\frac{\partial \phi_{s,j}}{\partial \theta} = w_{s,j} \sum_{i=0}^{N} \gamma_i r_i \left(\frac{\partial c_i}{\partial \theta}\right), \tag{C 12}$$

which is derived by taking the partial derivatives of equation (16) with respect to θ. In the above relation, $\partial c_N/\partial \theta = 0$, whereas $\partial c_0/\partial \theta$ is

$$\partial c_0/\partial \theta = (4\partial c_1/\partial \theta - \partial c_2/\partial \theta)/3. \tag{C 13}$$

We examine now the calculation of the sensitivity coefficients via the integration of the equations (C 10). The jacobian $\partial f/\partial Y$ is already available since its ith row is identical with the derivatives of the right-hand side ith equation (C 4) with respect to the variables c_{i-1}, c_i and c_{i+1}, whereas the jacobian $\partial f/\partial \theta$ is obtained by differentiating the equations (C 4) with respect to θ. It is noted that the sensitivity equations also have a tridiagonal form which is exploited in the solution of the corrector equations. When an integrator based on Gear's method like DASSL is used, it is possible to integrate efficiently the sensitivity equations together with the original ones by modifying certain parts of the integration algorithm. We shall not discuss here these modifications; we refer the interested reader to the paper of Caracotsios & Stewart (1985). Following the ideas of the latter authors, appropriate modifications of the DASSL code were carried out so that the original equations together with the sensitivity ones could be integrated accurately while incurring the minimum computational cost. The modified DASSL code was utilized in the parameter estimation. Our computational experience in this study has shown that the effort involved in deriving the sensitivity equations and in modifying DASSL was worthwhile.

References

Ames, W. F. 1977 *Numerical methods for partial differential equations*. New York: Academic Press.

Bard, Y. 1974 *Non-linear parameter estimation*. New York: Academic Press.

Brenan, K. E., Campbell, S. L. & Petzold, L. R. 1989 *Numerical solution of initial-value problems in differential-algebraic equations*. New York: North-Holland.

Briscoe, B. J. & Liatsis, D. 1992 *Rubber Chem. Technol.* (In the press.)

Briscoe, B. J., Liatsis, D. & Mahgerefteh, H. 1986 *J. Phys.* E **19**, 1039.

Briscoe, B. J., Liatsis, D. & Zakaria, S. 1990 *Meas. Sci. Technol.* **1**, 831.

Briscoe, B. J. & Mahgerefteh, H. 1984 *J. Phys.* E **17**, 483–487.

Briscoe, B. J. & Zakaria, S. 1990 *J. Mater. Sci.* **25**, 3017–3023.

Briscoe, B. J. & Zakaria, S. 1991 *J. Polymer Sci.* B **29**, 989–999.

Caracotsios, M. & Stewart, W. E. 1985 *Comp. chem. Engng* **9**, 359–365.

Crank, J. 1975 *Mathematics of diffusion*, 2nd edn. Oxford: Clarendon Press.

Gear, C. W. 1971 *Numerical initial value problems in ordinary differential equations.* Englewood Cliffs, N.J.: Prentice-Hall.

Koros, W. J., Paul, D. R., Fujii, M., Hopfenberg, H. B. & Stannett, V. 1977 *J. appl. Polymer Sci.* **21**, 2899.

Kreyszig, E. 1979 *Advanced engineering mathematics* A-62. New York: J. Wiley.

Petzold, L. R. 1983 A description of DASSL. A differential/algebraic system solver. In *Scientific computing* (ed. R. Stepleman), pp. 65–68. IMACS/North-Holland.

Prager, S. & Long, F. A. 1951 *J. Am. chem. Soc.* **73**, 4072.

Prescott, J. 1924 *Applied elasticity*, ch. IX. London: Longman.

Rennie, A. R. & Tabor, D. 1980 *Nature, Lond.* **286**, 372.

Received 12 March 1991; revised 14 October 1991; accepted 29 November 1991

PHILOSOPHICAL TRANSACTIONS OF THE ROYAL SOCIETY A MATHEMATICAL, PHYSICAL & ENGINEERING SCIENCES